Exosome-mediated crosstalk stimulated by liver fluke granulin promotes a microenvironment conducive to cholangiocarcinoma

Patpicha Arunsan[1,2,*], Apisit Chaidee[1,2,*], Christina J. Cochan[1], Victoria H. Mann[1], Toshihiko Tanno[3], Chutima Kumkhaek[4], Michael J. Smout[5], Shannon E. Karinshak[1], Rutchanee Rodpai[1,2], Javier Sotillo[5,6], Alex Loukas[5], Thewarach Laha[2], Paul J. Brindley[1*], Wannaporn Ittiprasert[1*]

[1] Department of Microbiology, Immunology & Tropical Medicine, & Research Center for Neglected Diseases of Poverty, School of Medicine & Health Sciences, George Washington University, Washington, D.C. 20037, USA

[2] Department of Parasitology, Faculty of Medicine, Khon Kaen University, Khon Kaen, 40002, Thailand

[3] Department of Surgery and the Institute of Human Virology, University of Maryland, Baltimore, MD 21201, USA

[4] Cellular and Molecular Therapeutics Laboratory, National Heart, Lungs and Blood Institute, National Institutes of Health, Bethesda, MD 20814 USA

[5] Centre for Molecular Therapeutics, Australian Institute of Tropical Health and Medicine, James Cook University, Cairns, QLD 4878, Australia

[6] Laboratorio de Helmintos, Laboratorio de Referencia e Investigación en Enfermedades Parasitarias, Centro Nacional de Microbiología, Madrid, España

*equal contribution

Correspondence: Wannaporn Ittiprasert, wannaporni@gwu.edu; Paul J. Brindley, pbrindley@gwu.edu

Abstract

Crosstalk between malignant and neighboring cells contributes to tumor growth. In East Asia, infection with fish-borne liver flukes is a major risk factor for cholangiocarcinoma (CCA). The liver fluke *Opisthorchis viverrini* secretes a growth factor, termed liver fluke granulin (*Ov*-GRN-1), a homologue of the human progranulin (huPGRN). Secreted *Ov*-GRN-1 contributes significantly to biliary tract fibrosis and morbidity during infection. Here, exosome-mediated transfer of mRNAs from a human cholangiocyte cell line following exposure to *Ov*-GRN-1 to naïve recipient cells was investigated. In addition, aiming to minimize the effects of endogenous human GRN, the gene encoding human granulin was inactivated in H69 line cholangiocytes by genome editing, and several huPGRN-depleted cell lines, termed ΔhuPGRN-H69 cells, were established. These mutant H69 cell lines, termed ΔhuPGRN-H69, exhibited >80% reduction in huPGRN transcription and protein expression, both within cells and within secreted exosomes. Profiles of exosomal RNAs (exRNA) from ΔhuPGRN-H69 cells for CCA-associated characteristics revealed a paucity of transcripts for estrogen- and Wnt-signaling pathways, peptidase inhibitors and tyrosine phosphatase related to cellular processes including oncogenic transformation. Exposure to *Ov*-GRN-1 induced CCA-specific mRNAs including mRNAs encoding MAPK/AKT pathway members. By comparison, estrogen, Wnt/PI3K and TGF signaling and other CCA pathway mRNAs were upregulated in wild type H69 exposed to Ov-GRN-1. Of these CCA-associated exRNAs, MAPK13 and SOX2 modified the microenvironment in naïve recipient cells co-cultured with exosomes from ΔhuPGRN-H69 exposed to *Ov*-GRN-1, and induced transcription of MAPK13 and SOX2 in naïve H69 cells. Crosstalk in response to liver fluke granulin promoted a CCA-specific program through RTK signaling via MAPK and Wnt/β-catenin which, in turn, established a CCA-conducive milieu.

Keywords

Granulin, *Opisthorchis viverrini*, cholangiocarcinoma, exosomal RNA, cancerous microenvironment, CCA mRNA intercellular transfer, crosstalk

Introduction

Cholangiocarcinoma (CCA) represents a diverse group of malignancies arising from the biliary epithelium. CCA is derived from cholangiocytes, which form the epithelial lining of both intrahepatic and extrahepatic bile ducts, except for those of the gallbladder. Many CCA are adenocarcinomas [1, 2]. The causative agent for many cancers remains obscure including non-liver fluke infection-associated CCA. By contrast, the principal risk factor in liver fluke-endemic regions is well established: infection with *O. viverrini* and related parasites [3-6]. Infection with *O. viverrini* is the principal risk factor for CCA in the Lower Mekong River Basin countries including Thailand, Lao PDR, Vietnam and Cambodia [5, 6]. It has been estimated that 10% of people chronically infected with liver flukes will develop CCA [7]. In regions endemic for opisthorchiasis, the prevalence of CCA can exceed 80 cases per 100,000 residents [8].

Helminth parasites communicate and interact at the host-parasite interface [9] Communication is facilitated by metabolic products secreted from the tegument and excretory tissues, including via exosomes [10]. The liver fluke *O. viverrini* releases numerous proteins and other metabolites [11], which influence host cells including cholangiocytes in diverse ways [12-15]. Whereas the full complement of metabolites released by this parasite remain generally to be investigated for roles of communication and disease, a secreted protein termed liver fluke granulin has been the focus of increasing investigation. *Ov*-GRN-1 is of human granulin, and like the human homologue stimulates cell proliferation, wound healing and has been suggested to contribute to the pathogenesis of opisthorchiasis [16-20].

Recently, we exploited this link to explore the role of the secreted growth factor termed liver fluke granulin (*Ov*-GRN-1) in pre-malignant lesions by undertaking programmed CRISPR/Cas9 knockout of the *Ov*-GRN-1 gene from the liver fluke genome. Deep sequencing of amplicon libraries from genomic DNA of gene-edited parasites revealed Cas9-catalyzed mutations within *Ov*-GRN-1. Gene editing resulted in rapid depletion of *Ov*-GRN-1 encoding transcripts and the *Ov*-GRN-1 protein. The infection resulted in markedly reduced disease even though gene-edited parasites colonized the biliary tract of hamsters and developed into adult flukes. These findings confirmed a role for *Ov*-GRN-1 in virulence of the hepatobiliary morbidity characteristic of opisthorchiasis [21]. In the present report, exosome-mediated transfer of mRNAs to naïve recipient H69 cholangiocytes from cholangiocytes following exposure to *Ov*-GRN-1 was investigated, including to recipient cells where the progranulin gene had been inactivated by CRISPR/Cas9 knockout. Exosome-mediated crosstalk in response to liver fluke granulin appeared to promote CCA-specific programs including via MAPK signaling that, in turn, established a microenvironment supportive of carcinogenesis.

Results

Programmed gene edited cell lines, ΔhuPGRN-H69

The CRISPR/Cas9 system was used to edit exon 2 of the human progranulin gene locus, a region encoding the N-terminus and part of the granulin/epithelin module (GEM) of huPGRN. H69 cells were transduced with pLV-huPGRNX2 virions at > 5 x 10^5 infective unit per ml (IFU) (Fig. 1A, B). One day later, transduced cells were transferred to culture medium supplemented with puromycin at increasing concentrations from 50 to 500 ng/ml, with the goal of enrichment of cells positive for expression of the puromycin resistance marker ($puro^R$)[22]. The daughter cell lines were termed ΔhuPGRN-H69. The three independent amplicon NGS libraries were

constructed (three biological replicates from cell culture passages number 20 in each case) were used to investigate the efficacy of on-target mutation knockout at huPGRN exon 2 in the ΔhuPGRN-H69 daughter lines.

Based on Ion Torrent NGS deep sequencing of the three amplicon libraries, 139,362, 107,683 and 179, 122 sequence reads were obtained and analyzed using the CRISPResso pipeline for prediction of on-target programmed gene cleavage and subsequent non-homologous end joining (NHEJ) mediated-repair, and insertion-deletion (INDEL) characteristics [23] compared with the wild type gene. Analysis of these sequenced reads using CRISPResso revealed the mutations in 32.3, 41.9 and 44.3% of the alleles from each of libraries, respectively. Similar INDEL profiles were seen in each library, with 6 bp and 2 bp deletions representing frequently observed deletion mutation alleles (Fig 1E) along with >0.08% 1 bp insertions and up to 10 bp deletions at the site of the expected Cas9-catalyzed double stranded chromosomal break (Fig 1C, D). These findings resembled earlier findings which had revealed preferred mutation patterns resulting from the chromosomal repair of CRISPR/Cas9 double stranded breaks by NHEJ in mammalian cells [24].

The surviving cells from three biological replicates were grown under puromycin selection. At that point, huPGRN transcript levels were reduced to only ~30% (24.83-34.56%) of levels of WT H69 cells (Fig. 2A). The INDELs on exon 2 of huPGRN DNA also affected the PGRN protein levels, which were only 21.45±2.34 % of the level of the WT progenitors H69 cells (normalized against the GAPDH reference) (Fig. 2B). These were significantly significant reductions (unpaired *t*-tests; $P < 0.0001$ in both).

Recovery of cell proliferation in huPGRN knock out cells following exposure to r*Ov*-GRN-1

To assess loss of cellular proliferation in H69 cells following mutation of the huPGRN gene by programmed CRISPR/Cas9 knockout, along with assessment of the mitogenic activity of r*Ov*-GRN-1, we monitored cell proliferation for more than 96 hours using the xCELLigence RTCA system [25]. This is a label-free cell-based assay system, which uses culture plates containing gold microelectrodes to non-invasively monitor the viability of cultured cells. The electrical impedance of the cell population in each well is measured by electrodes to provide quantitative real time information about the cell growth. During the assay, the impedance value of each well was automatically monitored. The rate of cell growth was determined by calculating the slope of the line between two given time points. Negative slope revealed that the cell index decreases with time and cells detach from the wells. Figure 2D presents the mean slope of three experiments performed in triplicate calculated at nine time points between 12-108 hours, for each of the wild type H69 parental cells and the ΔhuPGRN-H69 daughter cell lines. The cells were exposed to liver fluke granulin at 100 nM.

From 12 to 84 hours, the ΔhuPGRN-H69 cells showed significantly less proliferation (CI 75-95%; blue) as compared to the H69 cells (gray line, used for normalization as 100% CI). Following pulsing with r*Ov*-GRN-1, cell proliferation rates of ΔhuPGRN-H69 cells (red) were similar to those for H69 (black) over the first 24 hours . Recombinant *Ov*-GRN-1 activated cell proliferation in both H69 and ΔhuPGRN-H69, leading to higher cell indexes (CI), i.e. more cellular proliferation than control cells not exposed to r*Ov*-GRN-1. This trend was evident for both the H69 and mutant H69 cells during the entire array, >96 hours. Even though H69 cells exposed to r*Ov*-GRN-1 proliferated at higher levels than the gene edited cells during the12-84 h, their CI values were similar by 96 hours (CI ~100%). Intriguingly, the ΔhuPGRN-H69 cells

exposed to r*Ov*-GRN-1 exhibited even higher levels of proliferation (>200% CI) and survived until the termination of the assay at day 5 (Figure 2D).

Characterization of exosomes from H69 cholangiocytes

Exosome particles from culture supernatants of H69 cells were precipitated using an exosome isolation reagent (ThermoFisher). Subsequently, the exosomes were examined for expression of by western blot (WB) analysis targeting the hallmark exosome surface marker CD9 and CD81, using antibodies specific for CD9 and CD81. Signals at the expected sizes of 24 kDa and 26 kDa, respectively, confirmed the presence of the target markers (Fig. 3A). In addition, biochemical characterization using the Exosome Antibody Array platform revealed the presence of exosomal marker proteins: flotillin-1 (FLOT-1), intercellular adhesion molecule 1 (ICAM), ALG-2- interacting protein 1 (ALIX), CD81, epithelial cell adhesion molecule (EpCAM), Annexin V (ANXAS) and tumor susceptibility gene 101 (TSG101). Together, these findings confirmed the identity of the supernatant particles as exosomes released from the H69 cells. In addition, these purified exosomes were negative for cis-Golgi matrix protein (GM130) on Exosome Antibody Array, indicating the absence of contaminating cellular debris (Fig. 3B). Confocal microscopy revealed exosome particles surrounding DAPI-stained nuclei of the H69 cells following probing with anti-CD81 labeled with fluorophore 488 (green). The particle size distribution ranged from 55-80 nm (Fig. 3C).

CRISPR/Cas9 knockout of huPGRN negatively impacted exosome-located granulin

We validated the expression of huPGRN exosomal mRNA from three biological replicates of puromycin resistant H69 cells at passage number 20 in each case. There was only 7.2% (4.65-9.83%) differential GRN transcript from exRNA of ΔhuPGRN-H69 (Fig. 3D) compared with H69 derived-exosomes, after normalizing with GAPDH. Means were compared using unpaired *t*-test ($P < 0.0001$) by Prism software.

Moreover, the programmed mutation induced INDELs at exon 2 of huPGRN DNA (Fig. 1) also negatively impacted translation of the PGRN within the protein complement of the exosomes. There was 10.46±1.96% proteomic huPGRN detected from the ΔhuPGRN-H69 cell compared with H69 cells after normalization with GAPDH protein from cell lysate and exosome protein, respectively. The huPGRN protein expression revealed by WB using anti-GRN antibody (Abcam, Cambridge, MA, catalog no. ab 108608) (product size, 64 kDa) compared with anti-GAPDH antibody (Sigma-Aldrich, catalog no. G9545). The GAPDH protein levels from both cell lysate and exosomal protein showed redundant expression (product size, 36 kDa). The low The levels of huPGRN protein from cell lysate and secreted exosomes were significantly lower than with H69 cells (unpaired Student's *t*-test, $P<0.0001$) (Fig. 3E).

CCA-related mRNA profiles from exosomal RNAs of H69 versus ΔhuPGRN-H69 cells

The 88 gene target Cholangiocarcinoma (CCA) Prime PCR array (Bio-Rad) was used. The cDNA of pooled exRNAs from three biological replicates (RNase treated) was synthesized using iScript Advanced cDNA Synthesis Kit (Bio-Rad). The cDNA was directly applied into CCA mRNA coated-well of 96-well plate (one gene per well), the SYBR green fluorescent PCR as manufacturer's instruction was run in a real time thermal cycler (iQ5, Bio-Rad). The levels of each transcript were calculated by the Prime PCR Bio-Rad software compared with control cDNA (exosome derived-H69), as described. Each cDNA sample was run in triplicate (three array per samples).

The ΔhuPGRN-H69 exRNAs did not include transcripts for dihydropyrimidine dehydrogenase (DPYD), estrogen receptor 1 and 2 (ESR1 and ESR2, respectively), lysine [K]-specific demethylase 3A (KDM3A), lymphoid enhancer-binding factor-1 (LEF1), protein tyrosine phosphatase, non-receptor type 13 (PRIN13 which is Fas-associated phosphatase), serpin peptidase inhibitor, clade A, member 3 (SERRINA3), serpin peptidase inhibitor, clade E, member 2 (SERRPINE2) and SRY-related HMG-box 11 (SOX11) (Fig. 4), while these mRNA read as positive in the exRNA from H69 cells. Using the PrimePCR™ Assay Validation report (Bio-Rad) for these genes, DPYD, ESR1, ESR2, KDM3A and SOX11genes are known to be involved in pyrimidine catabolic enzymes, hormone binding, DNA binding and activation of transcriptions and activate transcription factor, respectively. LEF1encodeds a transcription factor that is involve in the Wnt signaling pathway. PTPN13 is a member of protein tyrosine phosphatase family which regulates a variety of cellular processes including oncogenic transformation [26]. The PRINA3 and SERPINA3 encode protease and peptidase inhibitors. The exogenous granulin, r*Ov*-GRN-1treatment recovered the expression of LEF1, SERRPINE2 and SOX11 in secreted exosomes (Fig. 4) with significant transcript induction in comparison with exRNA from H69 cells.

CCA pathways potentially impacted by liver fluke granulin-induced activation

There were seven exRNAs; annexin A3 (ANXA3), heparinase (HPSE), S100 calcium binding protein P (SP100P), carbonic anhydrase II (CA2), protein kinase C, theta (PRKCθ), thymidine phosphorylase (TYMP), mitogen-activated protein kinase 13 (MAPK13) that were not detected in exRNA-H69 (control). However, after r*Ov*-GRN-1treatment these genes were read as strongly positive SYBR green signals in the PrimePCR array (Bio-Rad) after normalization with reference genes (Fig. 4). The genes in family of calcium-dependent phospholipid-binding protein associated with cellular growth and signal transduction include ANXA3, CA2 and SP100P. The signal pathway(s) for extracellular matrix remodeling and angiogenesis were revealed from HPSE (enzyme that cleaves heparan sulfate proteoglycans to permit cell movement through remodeling of the extracellular matrix) and TYMP (angiogenic factor) exRNA expression. Two exosome transcripts, PRCKθ and MAPK13 involved in the MAPK signaling pathway were detected in ΔhuPGRN-H69 cell after r*Ov*-GRN-1activation. They were absent from exRNAs derived from H69 or ΔhuPGRN-H69 cells. Accordingly, our findings accord with the hypothesis that MAPK is a major pathway involved in cholangiocarcinogenesis associated with liver fluke infection [20, 27].

Moreover, six transcripts showed significant induction (4-6 differential transcript changes) in exosomes derived ΔhuPGRN-H69 cells, but change in exosomes derived H69 cell after r*Ov*-GRN-1treatment was not apparent. The ATP-binding cassette, sub-family C, member 1 and 4 (ABCC1 and ABCC4, respectively), calcium/calmodulin-dependent protein kinase II gamma (CAMK2G), interleukin-17 receptor A (IL17RA), lymphoid enhancer-binding factor 1(LEF1) and 8-oxoguanine DNA glycosylase (OGG1) exhibited significantly elevated transcript levels, >2 fold greater than levels in H69 cells.

Potential of endogenous granulin support mitogen O. viverrini granulin to induce the CCA tumorigenesis in cholangiocyte

To investigate the endogenous growth factor huPGRN that is potentially involved together with exogenous GRN which could mimic *in vivo* evidence of *Ov* infection, we also activated H69 with 100 nM r*Ov*-GRN-1for overnight in medium containing exosome depleted serum. The

exosome RNA was performed for exRNA transcript expression as mentioned above. Our results revealed 39 from 88 CCA related-gene profile including DPYD, ESR1, ESR2, LEF1, and SERPINA3 shown significant induction (≥2 folds change) comparing with exRNAs from H69 cells. Ten exRNAs including KDM3A, PTPN13, SERPINE2, and SOX11 (absent in ΔhuPGRN-H69) were expressed from both H69 and ΔhuPGRN-H69 cells after r*Ov*-GRN-1 activation. Another six genes are ERBB2, FBXW7, RRM1, SCD, SOX2 and ZNF827 encode epidermal growth factor, F-box protein, ribonucleotide reductase M1, stearoyl-CoA desaturase, and SOX family transcription factor and zinc finger protein 827. Most of these genes are involved in cancerous mechanism and malignancies as shown in Figure 4.

Twenty-nine CCA related-genes were increased from exosomes derived, r*Ov*-GRN--treated-H69 cells. These mRNA transcripts did not observe or non-significant induction in exRNAs from r*Ov*-GRN-1treated-ΔhuPGRN-H69 cells. The function of these genes was as follows: *1) cell structure*, including tubulin beta 2a (TUBB2A), mitochondrial ribosomal protein S6 (MRPS6), haptoglobin (HP), keratin19 (KRT19), actin 1 (ACTA1), breast cancer 1 (BRCA1) and chloride intercellular channel 5 (CLIC5); *2) enzymes*, peptidase inhibitor (SERRPINA3), phospholipase A2 (PLA2G2A), ornithine decarboxylase 1 (ODC1), natriuretic peptide B (NPPB) and o-6-methylguanine-DNA methyltransferase (MGMT); *3) transcription factor/signal transduction*, neuronal PAS domain protein 2 (NPAS2), msh home box1 (MSX1) and homeboxA9 (HOXA9) *4) growth factor*, insulin-link growth factor2 mRNA binding protein 3 (IGF2BP3), IGF2, epidermal growth factor receptor (EGFR); *5) Estrogen pathway signaling*, ESR1 and ESR2; *6) Wnt signaling*, homolog 7 (FZD7); *7) cell signaling/migration*, neuron navigator 2 (NAV2), chemokine (C-X-C-motif) receptor 4 (CXCR4) and cannabinoid receptor (CNR1); *8) TGF-beta signaling*, SMAD family member 4 (SMAD4); and *9) unknown function*, metadherin (MTDH).

Cholangiocyte cell line endocytose exosome particles *via* clathrin endocytosis mechanism

Extracellular exosomes have shown evidence that they can enter cells and deliver their cargo to the recipient cells [28]. To confirm the event of exosome internalization by recipient cells, we labeled the exosomes with PKH-26 red fluorescent cell linker kit (Sigma-Aldrich) before direct co-culture with H69 cells for 90 min. The endocytosis inhibitor reagent, Pitstop **was also included to block clathrin endocytosis mechanism of H69 cells. The cells were pre-incubated with** Pitstop for 15 min before adding PKH-26 labeled-exosomes. From our results, we observed that H69 start endocytosed the exosome particles early as 30 min, and success to endocytose ~90% of cell population within 90 min (Fig. 5). Far fewer cells endocytosed exosomes after exposure to Pitstop2.

Horizontal intercellular transfer exosomal RNAs from r*Ov*-GRN-1 activated-ΔhuPGRN-H69 donor cells to naïve recipient cells

To study the horizontal transfer of mRNA from donor cells, r*Ov*-GRN-1treated-ΔhuPGRN-H69 cell via exosomes to the naïve recipient cells either H69 or -ΔhuPGRN-H69 cells, we treated recipient cells with freshly prepared-deriving from r*Ov*-GRN-1treated-ΔhuPGRN-H69 cell for 18 h before co-culture with adherent recipient cells for 3, 6 and 24 hours. The genes of interest that present/induce after r*Ov*-GRN-1activation including MAPK13, SOX11, and SOX2 were investigated for cellular mRNA expression in recipient cells comparing with control group. The control group was untreated with exosomes derived-ΔhuPGRN-H69 cell.

From our experiment, we demonstrated that the exosomes carrying CCA related-mRNA from r*Ov*-GRN-1treated-ΔhuPGRN-H69 cell were functional and be able to stimulate the naïve cells for cellular transcript of the particular messages. After exosome co-culture, we observed the MAPK13 transcript induction for 3-6 hours from both naïve H69 cell with 300-512% different fold changes and ΔhuPGRN-H69 cells with 130 to 256% different fold change compared with the respective controls (indicated as 100% expression) (Fig. 5F). The MAPK13 transcript showed a high peak expression at 6 hours, after which it fell during the co-culture. However, at 24 h, the level of the MAPK13 transcript were still statistic significantly higher than the control group. The H69 cell was stimulated for MAPK13 transcript induction higher than ΔhuPGRN-H69 cell (Fig. 5F).

Similar findings were seen with the SOX2 transcript pattern for 3-24 hours from the recipient cell types. At 6 hours, SOX2 from H69 has shown ~1,024 folds change and ~150 folds change at 24 hrs. The SOX2 exRNA stimulated ΔhuPGRN-H69 cell quicker than in H69 cells showing more than 2,048 folds different after 3 h exosome co-culture. The SOX2 transcript shown statistic significantly higher than control cell in all time points (Fig. 5D). On the other hand, the stimulation of SOX11 transcript in recipient cells was success in only H69 cell after 6 hrs. The over expression of SOX11 at 6 h post co-culture shown over 10,000 folds changes, and ~5,000 folds changes at 24 hrs. Transcript level changes for SOX11 were not seen in ΔhuPGRN-H69 cells (Fig. 5E).

Discussion

A recent report charted the mutational profiles of ~500 human CCA tumors, including tumors from liver fluke infection positive- and non-fluke infection-associated cases [27]. Among the mutational differences between these epidemiologically and geographically distinct forms, the tumor clusters were distinguished by idiosyncratic patterns of genome-wide DNA hypermethylation, targeting either promoter CpG islands or promoter CpG shores, as well as differences in driver genes. Somatic mutations occur frequently in the tumor suppressor genes *p53* and *smad4* in *O. viverrini*–induced CCA whereas the genes encoding BRCA1 associated protein-1 and isocitrate dehydrogenases 1 and 2 are mutated frequently with CCA in regions not endemic for opisthorchiasis or clonorchiasis. The differences were consistent with a model where external carcinogenic agents and early epigenetic deregulation drive the nascent neoplasia in liver fluke infection positive CCAs whereas, by contrast, pioneering mutations such as in *BAP1* or *IDH1/2* loci or *FGFR2* gene rearrangements drive cholangiocarcinogenesis in many non-fluke infection-associated tumors. The investigators posit that, in this model [27], infection with the liver fluke induces global epigenetic deregulation in the presence of chronic inflammation, provoked by the mechanical damage inflicted by the feeding and by other activities of the parasite, including secreted factors such as liver fluke granulin, thioredoxin peroxidase, extracellular vesicles and others that modulate the host-pathogen interactions [11, 15, 20].

Human progranulin is a secreted, cysteine-rich glycoprotein that regulates cell division, survival, motility and migration. It has roles in development, wound repair, and cancer, and mutations in the progranulin gene are associated with a spectrum on neurological disorders [29]. In this present report, we investigated the exosome-mediated cellular crosstalk among cholangiocytes in response to liver fluke granulin. The human granulin gene (huPGRN) was disabled by CRISPR/Cas9, with the aim of masking the influence of endogenous granulin on exogenous liver

fluke granulin. Exosome-mediated crosstalk in response to liver fluke granulin appears to promote CCA-specific programs including via MAPK signaling that, in turn, establish a CCA-conducive microenvironment. *Ov*-GRN-1 is a paralogue of human granulin, and stimulates cell proliferation, wound healing and has been suggested to contribute to the pathogenesis of opisthorchiasis [16-20]. We have exploited this link to explore the role of the secreted growth factor termed liver fluke granulin (*Ov*-GRN-1) in pre-malignant lesions by undertaking programmed CRISPR/Cas9 knockout of the *Ov*-GRN-1 gene from the genome of *O. viverrini*. The infection with *Ov*-GRN-1 knockout worms resulted in markedly reduced disease, which confirmed the key role for this liver fluke granulin in hepatobiliary morbidity during opisthorchiasis [21].

Following the result of cell proliferation, xCELLigence assay in the ΔhuPGRN-H69 cell group revealed the cell progression more than the normal cell after r*Ov*-GRN-1 treatment for 24 hours and H69 cell were dead at 100 hours. We can say, if host cell have a role of endogenous growth factor gene together exogenous growth factor, *Ov*-GRN-1, may be attenuate the virulence during *O. viverrini* infection on the long term due to huPGRN and *Ov*-GRN-1 together may be affected to reduce or disrupt the functions in two growth factors in the normal cell. Examination of the CCA gene array revealed CCA genes to cooperate with the exosomes after exposure to r*Ov*-GRN-1 , both for H69 and ΔhuPGRN-H69 cells including highlighting the likely importance of signaling pathways related to intracellular communication --- after the naïve H69 and ΔhuPGRN-H69 cells were activated with exosomes of the mutant huPGRN-H69 cell treated with recombinant protein of exogenous growth factor, r*Ov*-GRN-1. We can suggest that the complement of human cholangiocytes can express the IL-6 and IL-8 through the TLR4-NF-kB and MAPK signaling pathways [30] which the MAPK pathway is the major of cholangiocarcinogenesis that activated by *Ov*-GRN during *O. viverrini* infection [16, 31]. For the CCA development providing indicate in the oncogenic signaling pathways [32], contribute on the many steps of carcinogenesis [33-35], including the Wnt/β-catenin signaling stimulated the pathology associated CCA [36], that the researcher suggested the Wnt/β-catenin signaling pathway can include in the inflammation that associated CCA and the Wnt/β-catenin pathway suppression influenced to inhibit CCA cell development [36]. Moreover, the cell apoptosis, cell growth, cell to cell interaction, and angiogenesis of CCA cells related with RTK signaling pathway that revealed the multiple kinases containing PI3K/AKT, Wnt/β-catenin, MAPK, and JAK/STAT signaling pathways [37-39]. And also, the previous study reported the GRN development effects to the activation of the MAPK signaling pathway [40], was highlighted as the upregulated gene in the hepatocellular carcinoma (HCC) and the targeted gene of microRNA□140□3p (miR□140□3p). Which the overexpression of miR□140□3p can disrupt the stimulation in the MAPK signaling pathway through inhibiting of GRN expression as resulting to the phosphorylation of ERK, p38, and c-Jun N-terminal kinase (JNK) was suppressed and effected to inhibit the migration and invasion of the HCC cells [41].

The fold change transcription levels of the MAK13 and SOX2 genes was seen to be up-regulated after the naïve H69 or mutant cells were exposed to, and presumably endocytosed, exRNA shed from ΔhuPGRN-H69 cells that had been exposed to *rOv*-GRN-1. On the other hand, SOX11 was up-regulated only in the WT H69 cells, when compared with the control group. Perturbation in the MAPK and Wnt signaling pathways that are activated in these cells may reflect the natural history of development of CCA [36], where SOX2 expression present in the precursor cells and supports self-renewal of a transformed cell [42-44] . SOX11 can play a role in the tumor cell

progression, in maintenance of the protein complex associated with the Wnt and angiogenesis signaling pathways [45-47].

In conclusion, we describe successful gene-editing in H69 cell by using Cas9 complexes with guide RNA complementary to human granulin by transduction with the lentiviral particles, the results revealed that gene-editing induced suppression of huPGRN expression in the transfected cell. In part of the intracellular communication revealed the relevant pathways in the CCA development that induced from the exogenous *Ov*-GRN-1 protein. Following programmed gene-editing, the lesion was apparently repaired via the NHEJ on the site of the huPGRN double-stranded break. The exogenous growth factor *Ov*-GRN-1 induces proliferation of human cholangiocytes and it also induces the expression of genes that participate in paracrine communication. It also induced changes reminiscent of those characteristic of malignant transformation, involving conserved signaling pathways. The findings indicated that cholangiocarcinogenesis may be O*v*-GRN-1 acting through the RTK signaling pathway and interconnection with the MAPK and Wnt/β-catenin pathways.

Materials and methods

Cell lines

The human nonmalignant immortalized cholangiocyte cell line (H69) was cultured in H69 complete medium; Ham's F12 nutrient mixture (25 μg/ml adenine, 5 μg/ml insulin, 1 μg/ml epinephrine, 0.62 μg/ml hydrocortisone, 1.36 μg/ml T3-T, and 10 ng/ml epidermal growth factor (EGF), Dulbecco's Modified Eagle Medium [DMEM] (Gibco), DMEM/F-12 (Sigma) media containing 10% fetal bovine serum (FBS) and 1× penicillin/streptomycin (pen/strep), as described [20, 48, 49]. H69 cells was maintained in humidified incubator with 5% CO_2 at 37ºC. H69 cells were *Mycoplasma* free as established using the Lookout Mycoplasma PCR detection kit (Sigma-Aldrich) and authenticated using STR profiling by ATCC before the start of this study (not shown).

Granulin knockout lines of H69 cholangiocytes

To mutate and disable the granulin gene to minimize or eliminate endogenous granulin expression from H69 that would bias the investigation of the effect of liver fluke granulin, we employed a pre-designed lentiviral CRISPR/Cas9 vector construct 'All in One CRISPR/Cas9 vector system (Sigma) containing guide RNA targeting human granulin, exon 2 which encodes granulin-epithelin precursor (GEP); 5'- cctgcaatctttaccgtctc of on chromosome 17: NC_000017.11 regions 44,345,086-44-353,106 driven by U6 promoter, elongation factor 1a promoter driving fusion proteins of the puromycin *N*-acetyl transferase from *Streptomyces alboniger* (puromycin resistance marker, $Puro^R$) [22] , Cas9 endonuclease from *Streptococcus pyogenes*, and green fluorescent protein (GFP), flanking with long tandem repeat (LTRs) of HIV-1 as integration sites (Fig. 1A). *E. coli* competent cells were transformed with this construct, termed pLV-huPGRNx2, and maintained in LB broth, 100 μg/ml ampicillin.

Several granulin gene-mutated H69 cell (termed ΔhuPGRN-H69) lines were established following pLV-huPGRNx2 virion-based transduction of the parent H69 cell line. The pLV-huPGRNx2 virion was produced by a MISSION™ lentiviral packaging kit (Sigma-Aldrich) and human 293T cells as producer cells using the FUGENE HD transfection reagent (Promega), as described [50]. The pooled culture supernatant containing pseudotyped virions was collected from 24 to 48 h after transfection of producer 293T cells. The culture supernatant was

centrifuged at 500 ×*g* for 10 min and filtered through a Millipore Steriflip-GP filter 0.45 µm pore size (Millipore). Virions were concentrated using Lenti-X concentrator (Takara Bio, CA) after which titer was measured by using Lenti-X-GoStix (Takara Bio, CA). To edit the exon 2 of the human granulin gene in H69 cells, ~350,000 H69 cells were exposed to 500 µl of pLV-huPGRNx2 virion (>10^5 infectious units IFU/ml) in 2.5 ml complete H69 medium in 6-well plates. Twenty-four hours later, the medium was replaced with medium supplemented with puromycin at 300 ng/ml for selection and enrichment of cells carrying the proviral form of the gene-editing construct. These gene edited cells were maintained in parallel with wild type (WT) H69 cells for 48 h, by which point all H69 cells had died. Surviving transduced-cells were cultured in complete H69 medium for 20 passages before genomic DNA extraction and genotyping. Between 5-10% of cells demonstrated survival and clonal amplification. There were three independent biological replicates to establish the puromycin-resistant, H69 knock-out cell line. The various concentrations, 50-400 ng/ml of puromycin have been optimized with H69 cells to induce cell death within 48 hours, before when employed 300 ng/ml puromycin for subsequent drug selection of the pLV-huPGRNx2 lentiviral virion transduced cells (data not shown).

Investigation for CRISPR/Cas9 induced mutations in exon 2 of human granulin by Ion Torrent Next Generation Sequencing

After pLV-huPGRNx2 transduction and high concentration of puromycin selection (300 ng/ml), the survival H69 cells were expanded with several cell culture passages. We amplified the targeted region of exon 2, huPGRN using the NGS primer pair; forward primer 5'-GACAAATGGCCCACAACACT-3' and reverse primer 5'-GCATAAATGCAGACCTAAGCCC-3' (Fig 1B) flanking double strand break (DSB). Genomic DNAs extracted from puromycin resistance-enriched ΔhuPGRN-H69 cells (pooled cells after passage 20) using DNAzol (Molecular Research Center). The DNA samples were proceeded for on-target insertion-deletion (indel) investigation by next generation sequencing (NGS), using the Ion Torrent Personal Genome Machine (ThermoFisher). The sequencing libraries were prepared from 10 ng DNA using the Ion Torrent Ampliseq kit 2.0-96 LV (ThermoFisher), following the manufacturer's instructions. The DNA was bar-coded using the Ion Xpress Barcode Adapters kit and quantified by quantitative PCR using the Ion Library TaqMan Quantitation Kit (ThermoFisher) after purification of libraries by Agencourt AMPure XP beads (Beckman). Emulsion PCR was performed using the Ion PGM Hi-Q View OT2 Kit and the Ion OneTouch 2 system (ThermoFisher). Template-positive ion sphere particles (ISPs) were enriched using the Ion Torrent OneTouchES. Enriched ISPs were loaded on a PGM 314R v2 chip and sequenced using the Ion PGM Hi-Q View Sequencing Reagents (ThermoFisher). Raw sequencing data were processed using the Torrent Suite software v5.0 (ThermoFisher), as well as the coverage analysis and variant caller (VC) v5.0 plugins. Processed reads were aligned to the human reference genome (hg38) [51]. All identified variants and the depth of coverage were visually confirmed by the Integrative Genomic viewer (IGV, Broad Institute, MIT, Cambridge, MA). The number of reads filtered out by post processing was 9.0%. Average read length was 176 bp. The filtered sequences were converted into fastq format and analyzed for non-homology end joining (NHEJ) mediated mutations by CRISPResso [23, 52]. Sequence reads were compared to the reference PCR sequence of the wild type *huPGRN* gene, GenBank accession M75161.1 (Fig. 1C, D, E).

Assessment of cell proliferation

We assessed the proliferation of H69 and ΔhuPGRN-H69 cells after 100 nM of recombinant *Ov*-GRN-1 (r*Ov*-GRN-1) [16, 20] treatment using impedance-based xCELLigence real time cell analysis (RTCA) system (ACEA Biosciences, San Diego, CA). The peptide r*Ov*-GRN-1was concentrated using Centripep with cut-off 3 kDa (Eppendorf) and resuspended in low salt solution, Opti-MEM. The absorbance at 205 nm and concentration of r*Ov*-GRN-1 was determined by using a Nanodrop 2000c spectrophotometer (ThermoFisher) [53]. Five thousand cells/well were seeded in 16 well-E-plates (ACEA) in H69 complete media. The E-plate was placed on xCELLigence station inside the incubator (37°C, 5% CO_2) and changes in impedance reflecting cell adhesion and proliferation record at intervals of 20 min for 24 h. On the following day, the medium was removed and replaced with H69 complete medium supplemented with r*Ov*-GRN-1 at 100 nM. Cellular proliferation was monitored for 96 hours, with data for the wild type H69, r*Ov*-GRN-treated H69, and ΔhuPGRN-H69 with and without r*Ov*-GRN-1treatment displayed as change of impedance (Cell Index) over time, normalized to wild type H69 (reference cell line in this assay) by RTCA Software 1.2 (ACEA) [25].

Isolation and characterization of exosomes

The WT-H69 or ΔhuPGRN-H69 cells were treated with 100 nM r*Ov*-GRN-1 in H69 complete media with 10% exosome depleted-FBS. Forty-eight hours later, were harvested the supernatant from cell culture of H69 with or without, and ΔhuPGRN-H69 with or without liver fluke granulin. The supernatants were collected at 48 h following addition of r*Ov*-GRN-1, then centrifuged at 2,000 ×*g* for 15 minutes to remove cells and cellular debris. The supernatant was filtered through a 0.22 μm pore size sterile filter (Millipore, Billerica, MA), mixed with 0.5 volume of Tissue culture total exosome isolation reagent (Invitrogen, catalog no. 4478359), and incubated for 16 h at 4°C. Thereafter, following centrifugation at 10,000 ×*g* at 4°C for 60 min, the exosome pellet was re-suspended in 1×PBS [54]. Exosomes were used in co-culture assay and also exosomal RNA and protein were extracted using the Total Exosome RNA and Protein Isolation kit (ThermoFisher) according to the manufacturer's protocols. About 10 μg of the exosomal protein was separated on gradient (4-12%) SDS-PAGE gel and followed by transfer to nitrocellulose membrane (Bio-Rad). After blocking with 5% skim milk powder in Tris-buffered saline (TBS)-Tween for 60 min, the membrane was incubated with specific antibody against CD9 and CD81 (Abcam, catalog no. ab58989), followed (after washing) by anti-rabbit HRP-linked secondary antibody (DAKO Corporation catalog no. P0448) diluted 1 in 2,000. Signals from ECL substrate were detected by chemiluminescence (Amersham Bioscience, Uppsala, Sweden).

The identification of protein markers on the isolated exosomes was undertaken using the commercially available Exo-Check Exosome Ab Array kit (System Biosciences, Palo Alto, CA), as described by the manufacturer. The membrane was developed with SuperSignal West Femto Maximum Sensitivity Substrate (Thermo Fisher Scientific) and analyzed using a ChemiDoc imager (Bio-Rad) [55] [56]).

For immunofluorescence staining of exosomes, the H69 cells were cultured in glass slide chamber overnight before fixed at 4°C in ice-cold methanol for 10 min, washed 3 times in phosphate-buffered saline (PBS), and then permeabilized in 0.1% Triton X-100/PBS for 10 min at room temperature. Nonspecific binding was blocked with 0.5% Tween-20/PBS containing 1% bovine serum albumin (BSA) for 30 min. The primary antibodies against fluoroflore-488

labelled-CD81 was incubated for 60 min at room temperature. The incubated cells were washed in PBS. Before visualization by confocal microscope, we stained the cell nucleus with DAPI. The exosome particles were observed in H69 cytoplasm, ranging in size from ~ 40 to ~100 nm.

Quantitative real time PCR

Total RNA and exosomal RNA either from wtH69 or ΔhuPGRN-H69 cells were isolated using RNAzol (Molecular Research Center, Inc.) or total exosome RNA isolation kit (ThermoFisher) following the manufacturer's instructions. One microgram of RNA was treated for DNase, then used for reverse transcription by an iScript cDNA synthesis kit (Thermo Fisher Scientific). Real time PCR was performed in ABI7300 Real time PCR machine using the SsoAdvanced Universal SYBR Green Supermix (Bio-Rad). The PCR reaction consisted of 5 µl SsoAdvance SYBR Green PCR master mix, 0.5 µl of 10 µM forward and reverse primers, and 2 µl of 5 times diluted template cDNA in a total volume of 10 µl. The thermal cycle was initiation cycle at 95°C for 30 sec followed by 40 cycles of annealing at 55°C for 1 min. Samples were analyzed in at least 3 biological replicates (various cell passages) and in typical reactions. The human glyceraldehyde-3-phosphate dehydrogenase (GAPDH) transcript was run parallel with human granulin (huPGRN) and used for gene normalization. The differential granulin transcript fold change was calculated by formula 2^{-ddCt} [57]. The specific primers for huPGRN (Fig. 1B) and GAPDH are as follows: PGRN-F: 5'-atgataaccagacctgctgcc-3', PGRN-R: 5'-aaacacttggtacccctgcg-3', GAPDH-F; 5'-tgtagttgaggtcaatgaaggg-3' and GAPDH-F 5'- tgtagttgaggtcaatgaaggg-3'. The means and standard deviations of differential transcript expression were calculated by independent Student's *t*-tests using GraphPad Prism software (La Jolla, CA).

Western blot

The protein lysate or exosomal protein from of WT H69 and ΔhuPGRN-H69 cells were prepared using M-PER mammalian protein extraction reagent (ThermoFisher) or exosome protein isolation kit (ThermoFisher, catalog no. 4478545) following the manufacturer's protocols. Protein concentration of samples was determined using the Bradford assay [58]. Ten micrograms of cell lysate or 20 µg of exosomal protein was separated on gradient SDS-polyacrylamide gel (4-12% Bis-Tris, Invitrogen) and transferred to nitrocellulose membrane (Trans-Blot Turbo, Bio-Rad). Each membrane was investigated by enhanced chemiluminescence (ECL) substrate (GE Healthcare) using first antibodies against huPGRN (Abcam, catalog no. ab 108608) or human GAPDH (hGAPDH) (Sigma-Aldrich, catalog no. G9545) and HRP conjugated-secondary antibodies. The expression level of huPGRN protein from cell lysate or exosomes were imaged and analyzed using the FluroChem system (Bio-techne, Minneapolis, MN). Relative expression levels of huPGRN protein were investigated after GAPDH level normalization and differences compared using independent Student's *t*-tests.

Cholangiocarcinoma (CCA) gene expression panel analysis

To investigate the CCA gene expression profile from exosomes derived-r*Ov*-GRN-1-treated H69, we used a predesigned Cholangiocarcinoma Pathway Panel (88 targets) (PrimePCR, Bio-Rad, Hercules, CA, catalog no. 100-2531). One microgram of total RNA from each exosome sample was converted to cDNA (Supermix iScript kit, Bio-Rad). A one in 10 dilution of cDNA was used for qPCR reaction mixture with final concentration of 1× SsoAdvanced universal SYBR super mix (Bio-Rad) and 1×PrimePCR assays for the designated target. Reactions were performed in three technical replicates at 10 µl final volume, using the iQ5 real time PCR system

(Bio-Rad) starting with activation at 95°C for 2 min, followed by 40 cycles of denaturation at 95°C, 5 s, and annealing/elongation at 60°C, 30 s. Specificity of target amplification was confirmed by melting-curve analysis. Controls for evaluating reverse transcription performance, RNA quality, genomic DNA contamination and PCR reaction performance were included from the array kit (Bio-Rad). The reference genes, TBP, GAPDH, and HPRT1 assay for relative gene expression analysis to normalize for variation in the amount of input mRNA between samples were included. The DNA template serve as a positive real-time PCR control for the corresponding gene assay. The differential fold change for the target genes was analyzed by PrimePCR Analysis Software (Bio-Rad).

Uptake of exosomes by cholangiocytes

To investigate whether r*Ov*-GRN-1 treated-H69 use the exosomal route to communicate CCA-conducive mRNAs to adjacent naïve cells, exosomes were labeled with the PKH26 Fluorescent cell linker kit (Sigma-Aldrich), which enables monitoring of exosome uptake and other nanoparticles in other cells [59, 60]. In brief, isolated exosomes from culture media were re-suspended in one ml of diluent C (an aqueous solution designed to maintain cell viability with maximum dye solubility and staining efficiency)[61]. Subsequently, 4 µl of PKH26 was diluted in another 1 ml diluent C. The samples were mixed gently and incubated for 5 min (periodic mixing), after which 2 ml 1% bovine serum albumin (BSA) was added to bind the excess dye. The mixture containing PKH26-stained exosomes was subjected to precipitation using Tissue culture exosome isolation reagent (ThermoFisher), as above, after which the exosomes were suspended in H69 complete medium and co-cultured with. H69 or ΔhuPGRN-H69 cells with at 80-90% confluency in cell culture 4 wells of poly-lysine coated cover slide chamber (Lab-Tek II), the negative control group was co-cultured with exosomes without PKH26 staining. After cells incubation with PKH26-labeled exosomes for 90 min at 37ºC in 5% CO_2, cells were stained with NucBlue Live Cell Stain ReadyProbes (Invitrogen) following the protocol and visualized the staining by confocal fluorescence microscopy (Zeiss Cell Observer SD Spinning Disk Confocal Microscope, Carl Zeiss Microscopy, Thornwood, NY). A negative control of endocytosis inhibition was included, which involved addition of Pitstop 2, endocytosis clathrin inhibitor (Abcam, catalog no. ab120687) [62] at 30 µM to recipient cells for 15 min, before co-culture with labeled-exosomes.

Functional CCA mRNA horizontally intercellular transfer via exosome

To demonstrate that the CCA mRNAs carrying by exosome derived-r*Ov*-GRN-1treated-ΔhuPGRN-H69 cells were endocytosed and function inside the naïve H69 cells. We co-cultured the PKH-26 stained-exosomes with recipient cells; WT-H69 or ΔhuPGRN-H69 cells. Briefly, 5×10^4 H69 or ΔhuPGRN-H69 cells were seeded into a poly-L-lysine coated wells of a 24-well plate and maintained overnight in H69 complete medium [63]. Thereafter, exosome particles (~6.25 µg) were added into each well, after which cells were collected at 3, 6 and 24 h. Cellular RNA was isolated as above, cDNA reverse transcribed using the iScript cDNA synthesis system (ThermoFisher), and levels of mRNA of target genes including MAPK13, SOX2, SOX11, ERBB2, PTPN13, and β-catenin established by RT-PCR, using SYBR Green labeling (SsoAdvance Master Mix, Bio-Rad). The specific primers are following: MAPK13 (forward: 5'-gagaaggtggccatcaagaa-3' and reverse: 5'-gtcctcattcacagccaggt-3') [64], SOX2 (forward: 5'-atgcacaactcggagatcag-3 and reverse 5'-tgagcgtcttggttttccg-3') [63], SOX11 (forward: 5'-gggccccagatggaaggtttgaa-3' and reverse 5'-gcattgagtctgctttgccacca-3') [65], ERBB2 (forward: 5'-cctctgacgtccatcatctc-3' and reverse: 5'-atcttctgctgccgtcgctt-3')[66], PTPN13 (forward: 5'-

caaaggtgatcgcgtccta-3' and reverse: 5'-cgggacatgttctttagatgtt-3') [26], and β-catenin (forward: 5'-aaaatggcagtgcgtttag-3' and reverse: 5'-tttgaaggcagtctgtcgta-3') [67]. The negative controls, non-exosome treated cells and exosome derived-ΔhuPGRN-H69 cell (without r*Ov*-GRN-1) were included to confirm that the high expression of CCA mRNAs were not artifacts.

Statistical analysis

Statistical analysis was performed using GraphPad Prism 8 software (GraphPad Software Inc). One-way ANOVA was used for every comparison between knockout genotypes versus wild type including before and after r*Ov*-GRN-1treatment. Multiple comparison measure ANOVA was used for cell growth curves comparison. Values of $P < 0.05$ were considered to be statistically significant. Cell index (CI) assays were performed in triplicate. CI was automatically registered by the software RTCA, ACEA Biosciences Inc., San Diego, CA, USA. Means ± SD are indicated, plotted using GraphPad Prism 8 (GraphPad Software, San Diego, CA).

Acknowledgements

We thank Drs. Griffin P. Rodgers, NIDDK, National Institutes of Health (NIH) and Yang Liu, Institute of Human Virology, School of Medicine, University of Maryland for support with exosome studies and Ion Torrent-based deep sequencing. PA was supported by the Ph.D. program at the Faculty of Medicine, Khon Kaen University and the Thailand Research Fund through the Royal Golden Jubilee Ph.D. Program, award number PHD/0111/2557 (PA, TL). We acknowledge support from award R01CA164719 (TL, AL, PJB) from the National Cancer Institute (NCI), NIH. The content is solely the responsibility of the authors and does not necessarily represent the official views of the Thailand Research Fund, the NCI or the NIH.

Figure legends

Figure 1. Programmed CRISPR/Cas9 mutation of the human progranulin gene in a cholangiocyte cell line. Panel A. Linear map of a pre-designed lentiviral construct containing codon-optimized Cas9 protein; gRNA targeting human granulin exon2 (red bar) and puromycin-resistant protein is expressed from a single vector. The human U6 promoter and T7 promoter were used for driven gRNA and fusion puromycin resistant (dark gray bar) and Cas9 (green bar) transcription, also the 5' and 3' long terminal repeats (LTR) of lentiviral vector derived from HIV-1 (light gray blocks). **Panel B.** Schematic of the partial human granulin gene precursor (GRN) on chromosome 17: NC_000017.11 regions 44,345,086-44,353,106 (8,021bp) and protein structure. Nucleotide sequence in exon2 encoded N-terminal and partial of granulin/epithelin module (GEM) indicating locations of gRNA (4,417-4,438 nt; red colored-letter) predicted double-stranded break (DSB) (red arrow). **Panel C, D, and E.** INDEL mutations resulting from gene-edited targeting exon2 of GRN in H69 cell. The mutants H69 cells (gRNA, Cas9, and puromycin integrated-cells), were survived after puromycin treatment (up to 300 ng/ml) and while the wild type H69 cells were completely dead. On-target gene repairs on exon2 of GRN locus were sequenced by Ion Torrent System and analyzed by CRISPResso. Frequency distribution of **Panel C** position-dependent insertions (red bars) and **Panel D** deletion (magenta bars) sizes; these varied from point mutations to 5 bp adjacent to the DSB. **Panel E.** The examples of mutations; 2 and 6 bp deletions, 1 bp insertion and substitutions comparing with the reference sequence. Three biological repeats were undertaken, and the numbers of reads and efficiency of gene editing were: Biological 1, 140,384 reads, 12.32% indels; biological 2, 93,689 reads, 10.94% indels; biological 3, 152,661 reads, 13.27% indels.

Figure 2. Characterization of exosomes shed from H69 cholangiocytes, the huPGRN mRNA and protein expression levels, and the proliferative effect of recombinant liver fluke granulin, r*Ov*-GRN-1. Panels A and B. Reduction of human GRN transcription levels from ΔhuPGRN-H69 cell RNA; red bars (~70%) comparing with WT H69 (black bars). The GRN differential transcript after normalization with human GAPDH gene; mean ±SD, n = 3 (biological replicates); $p < 0.0001$ (****) by unpaired *t*-test. Diminished level of hPGRN protein revealed by western blot analysis using anti-PGRN antibody compared with anti-GAPDH antibody. The reduction of PGRN in ΔhuPGRN-H69 cells (red bars) was ~80%. The GAPDH protein levels were stable. These decreased levels of PGRN protein were significantly different from WT H69 (black bars); n = 3 (biological replicates); $p < 0.0001$ (****) by unpaired Student's *t*-test. **Panel C.** The low percentage of relative cell growth index of ΔhuGRN-H69 cells (blue line) compared with WT H69 cells (gray line). The growth index of ΔhuGRN-H69 was normal after *Ov*-GRN treatment (100 nM) for 12 hours (red line) as *Ov*-GRN treated-WT H69 (black line). The ΔhuGRN-H69 continued to grow under *Ov*-GRN treatment for up to 100 hours , while growth of wild type H69 had slowed at 24 hours and all the cells died by 100 hours.

Figure 3. Exosome derived H69 cell characterization and PGRN expression. Panels A, B. Characterization of exosomes from H69 cells by western blot for the exosome-specific markers, CD9 and CD81. The vesicle composition was determined using an Exosome Antibody Array. Dark spots indicate presence of the marked protein. Absence of a spot for GM130 indicates absence of cellular contaminants (**panel C**). The visualization of exosome particles in H69 cell cytoplasm were revealed by confocal microscopy with anti-CD81l labelled with fluorophore 488 (green) with a size distribution between 40-100 nm ; DAPI-stained nuclei (blue). The exosomal RNA and cell lysate protein from ΔhuPGRN-H69 showed ~90% reduction (**panels D, E**, red lines) after normalization with huGAPDH and comparison with H69 (black). The levels of PGRN were significantly reduced; unpaired *t*-test, $p < 0.0001$ (****), n = 3.

Figure 4. The cholangiocarcinoma (CCA) related-gene array analysis. Panel A. The CCA gene records of ΔhuGRN-H69 cells with and without exposure to recombinant *Ov*-GRN-1, compared with H69 exosomal RNA. The heat map was plotted using GraphPad Prism 8 for exosomal CCA mRNA expression profiles of the ΔhuGRN-H69, r*Ov*-GRN +H69, r*Ov*-GRN + ΔhuGRN+H69 treatment groups of cells, with differential fold changes in transcription, from 0-15-fold. The '1' indicates baseline level expression, and '0' indicated the absence of expression.

Figure 5. Confirmation of uptake of extracellular exosomes and paracrine transfer of mRNA from donor cells to the naïve recipient cells. Panel A. Fifty-thousand naïve H69 or ΔhuGRN-H69 cells were seeded into 4-well chambers, coated with poly-L-Lysine and incubated at 37 °C for overnight. Subsequently the medium was replaced, and the cells incubated cells for 90 min, at which point nuclei were stained with NucBlu Live Cell Stain ReadyProbe reagent (blue). A negative control group, which was not co-cultured with the labeled exosomes, was included. Merged (right panel) left panel with bright field. Magnification, 40×; scale bar, 10 µm**.** **Panel B.** Confirmation that exRNAs secreted from donor cells have been endocytosed and entered the target cells. The modifying of the gene expression microenvironment in naïve cell were confirmed by analysis of several informative target genes - SOX2, SOX11 and MAPK13 at various time points (0-24 hours). With the responses likely to have resulted from regulation by the exosomal RNA (exRNA).

693
694 **References**

695 1. Sirica AE, Gores GJ, Groopman JD, Selaru FM, Strazzabosco M, Wei Wang X, et al.
696 Intrahepatic Cholangiocarcinoma: Continuing Challenges and Translational Advances.
697 Hepatology. 2019;69(4):1803-15. Epub 2018/09/27. doi: 10.1002/hep.30289. PubMed PMID:
698 30251463; PubMed Central PMCID: PMCPMC6433548.
699 2. Khan AS, Dageforde LA. Cholangiocarcinoma. Surg Clin North Am. 2019;99(2):315-35.
700 Epub 2019/03/09. doi: 10.1016/j.suc.2018.12.004. PubMed PMID: 30846037.
701 3. Shin HR, Oh JK, Masuyer E, Curado MP, Bouvard V, Fang YY, et al. Epidemiology of
702 cholangiocarcinoma: an update focusing on risk factors. Cancer Sci. 2010;101(3):579-85. Epub
703 2010/01/21. doi: 10.1111/j.1349-7006.2009.01458.x. PubMed PMID: 20085587.
704 4. Fedorova OS, Kovshirina YV, Kovshirina AE, Fedotova MM, Deev IA, Petrovskiy FI, et
705 al. Opisthorchis felineus infection and cholangiocarcinoma in the Russian Federation: A review
706 of medical statistics. Parasitol Int. 2017;66(4):365-71. Epub 2016/07/31. doi:
707 10.1016/j.parint.2016.07.010. PubMed PMID: 27474689.
708 5. Sripa B, Kaewkes S, Sithithaworn P, Mairiang E, Laha T, Smout M, et al. Liver fluke
709 induces cholangiocarcinoma. PLoS Med. 2007;4(7):e201. Epub 2007/07/12. doi:
710 10.1371/journal.pmed.0040201. PubMed PMID: 17622191; PubMed Central PMCID:
711 PMCPMC1913093.
712 6. Humans IWGotEoCRt. Biological agents. Volume 100 B. A review of human
713 carcinogens. IARC Monogr Eval Carcinog Risks Hum. 2012;100(Pt B):1-441. PubMed PMID:
714 23189750.
715 7. Sithithaworn P, Yongvanit P, Duenngai K, Kiatsopit N, Pairojkul C. Roles of liver fluke
716 infection as risk factor for cholangiocarcinoma. J Hepatobiliary Pancreat Sci. 2014;21(5):301-8.
717 Epub 2014/01/11. doi: 10.1002/jhbp.62. PubMed PMID: 24408775.
718 8. Khan SA, Tavolari S, Brandi G. Cholangiocarcinoma: Epidemiology and risk factors.
719 Liver Int. 2019. Epub 2019/03/10. doi: 10.1111/liv.14095. PubMed PMID: 30851228.
720 9. Maizels RM, Smits HH, McSorley HJ. Modulation of Host Immunity by Helminths: The
721 Expanding Repertoire of Parasite Effector Molecules. Immunity. 2018;49(5):801-18. Epub
722 2018/11/22. doi: 10.1016/j.immuni.2018.10.016. PubMed PMID: 30462997; PubMed Central
723 PMCID: PMCPMC6269126.
724 10. Coakley G, Maizels RM, Buck AH. Exosomes and Other Extracellular Vesicles: The
725 New Communicators in Parasite Infections. Trends Parasitol. 2015;31(10):477-89. Epub
726 2015/10/05. doi: 10.1016/j.pt.2015.06.009. PubMed PMID: 26433251; PubMed Central PMCID:
727 PMCPMC4685040.
728 11. Mulvenna J, Sripa B, Brindley PJ, Gorman J, Jones MK, Colgrave ML, et al. The
729 secreted and surface proteomes of the adult stage of the carcinogenic human liver fluke
730 Opisthorchis viverrini. Proteomics. 2010;10(5):1063-78. Epub 2010/01/06. doi:
731 10.1002/pmic.200900393. PubMed PMID: 20049860; PubMed Central PMCID:
732 PMCPMC3038172.
733 12. Sripa B. Pathobiology of opisthorchiasis: an update. Acta Trop. 2003;88(3):209-20. Epub
734 2003/11/13. PubMed PMID: 14611875.
735 13. Chaiyadet S, Smout M, Laha T, Sripa B, Loukas A, Sotillo J. Proteomic characterization
736 of the internalization of Opisthorchis viverrini excretory/secretory products in human cells.
737 Parasitol Int. 2017;66(4):494-502. Epub 2016/02/14. doi: 10.1016/j.parint.2016.02.001. PubMed
738 PMID: 26873540; PubMed Central PMCID: PMCPMC5149449.

14. Chaiyadet S, Smout M, Johnson M, Whitchurch C, Turnbull L, Kaewkes S, et al. Excretory/secretory products of the carcinogenic liver fluke are endocytosed by human cholangiocytes and drive cell proliferation and IL6 production. Int J Parasitol. 2015b;45(12):773-81. doi: 10.1016/j.ijpara.2015.06.001. PubMed PMID: 26187786; PubMed Central PMCID: PMCPMC4912216.

15. Chaiyadet S, Sotillo J, Smout M, Cantacessi C, Jones MK, Johnson MS, et al. Carcinogenic Liver Fluke Secretes Extracellular Vesicles That Promote Cholangiocytes to Adopt a Tumorigenic Phenotype. J Infect Dis. 2015a;212(10):1636-45. doi: 10.1093/infdis/jiv291. PubMed PMID: 25985904; PubMed Central PMCID: PMCPMC4621255.

16. Smout MJ, Laha T, Mulvenna J, Sripa B, Suttiprapa S, Jones A, et al. A granulin-like growth factor secreted by the carcinogenic liver fluke, Opisthorchis viverrini, promotes proliferation of host cells. PLoS Pathog. 2009;5(10):e1000611. Epub 2009/10/10. doi: 10.1371/journal.ppat.1000611. PubMed PMID: 19816559; PubMed Central PMCID: PMC2749447.

17. Bansal PS, Smout MJ, Wilson D, Cobos Caceres C, Dastpeyman M, Sotillo J, et al. Development of a Potent Wound Healing Agent Based on the Liver Fluke Granulin Structural Fold. J Med Chem. 2017;60(10):4258-66. Epub 2017/04/21. doi: 10.1021/acs.jmedchem.7b00047. PubMed PMID: 28425707.

18. Dastpeyman M, Bansal PS, Wilson D, Sotillo J, Brindley PJ, Loukas A, et al. Structural Variants of a Liver Fluke Derived Granulin Peptide Potently Stimulate Wound Healing. J Med Chem. 2018;61(19):8746-53. Epub 2018/09/06. doi: 10.1021/acs.jmedchem.8b00898. PubMed PMID: 30183294.

19. Haugen B, Karinshak SE, Mann VH, Popratiloff A, Loukas A, Brindley PJ, et al. Granulin Secreted by the Food-Borne Liver Fluke Opisthorchis viverrini Promotes Angiogenesis in Human Endothelial Cells. Front Med (Lausanne). 2018;5:30. Epub 2018/03/06. doi: 10.3389/fmed.2018.00030. PubMed PMID: 29503819; PubMed Central PMCID: PMCPMC5820972.

20. Smout MJ, Sotillo J, Laha T, Papatpremsiri A, Rinaldi G, Pimenta RN, et al. Carcinogenic Parasite Secretes Growth Factor That Accelerates Wound Healing and Potentially Promotes Neoplasia. PLoS Pathog. 2015;11(10):e1005209. Epub 2015/10/21. doi: 10.1371/journal.ppat.1005209. PubMed PMID: 26485648; PubMed Central PMCID: PMC4618121.

21. Arunsan P, Ittiprasert W, Smout MJ, Cochran CJ, Mann VH, Chaiyadet S, et al. Programmed knockout mutation of liver fluke granulin attenuates virulence of infection-induced hepatobiliary morbidity. Elife. 2019;8. doi: 10.7554/eLife.41463. PubMed PMID: 30644359; PubMed Central PMCID: PMCPMC6355195.

22. Vara JA, Portela A, Ortin J, Jimenez A. Expression in mammalian cells of a gene from Streptomyces alboniger conferring puromycin resistance. Nucleic acids research. 1986;14(11):4617-24. Epub 1986/06/11. doi: 10.1093/nar/14.11.4617. PubMed PMID: 3714487; PubMed Central PMCID: PMCPMC311469.

23. Pinello L, Canver MC, Hoban MD, Orkin SH, Kohn DB, Bauer DE, et al. Analyzing CRISPR genome-editing experiments with CRISPResso. Nat Biotechnol. 2016;34(7):695-7. Epub 2016/07/13. doi: 10.1038/nbt.3583. PubMed PMID: 27404874; PubMed Central PMCID: PMCPMC5242601.

24. Shen MW, Arbab M, Hsu JY, Worstell D, Culbertson SJ, Krabbe O, et al. Predictable and precise template-free CRISPR editing of pathogenic variants. Nature. 2018;563(7733):646-51. Epub 2018/11/09. doi: 10.1038/s41586-018-0686-x. PubMed PMID: 30405244.
25. Ke N, Wang X, Xu X, Abassi YA. The xCELLigence system for real-time and label-free monitoring of cell viability. Methods Mol Biol. 2011;740:33-43. Epub 2011/04/07. doi: 10.1007/978-1-61779-108-6_6. PubMed PMID: 21468966.
26. Revillion F, Puech C, Rabenoelina F, Chalbos D, Peyrat JP, Freiss G. Expression of the putative tumor suppressor gene PTPN13/PTPL1 is an independent prognostic marker for overall survival in breast cancer. Int J Cancer. 2009;124(3):638-43. Epub 2008/11/13. doi: 10.1002/ijc.23989. PubMed PMID: 19004008; PubMed Central PMCID: PMCPMC2740876.
27. Jusakul A, Cutcutache I, Yong CH, Lim JQ, Huang MN, Padmanabhan N, et al. Whole-Genome and Epigenomic Landscapes of Etiologically Distinct Subtypes of Cholangiocarcinoma. Cancer Discov. 2017;7(10):1116-35. Epub 2017/07/02. doi: 10.1158/2159-8290.CD-17-0368. PubMed PMID: 28667006; PubMed Central PMCID: PMCPMC5628134.
28. Hu L, Wang J, Zhou X, Xiong Z, Zhao J, Yu R, et al. Exosomes derived from human adipose mensenchymal stem cells accelerates cutaneous wound healing via optimizing the characteristics of fibroblasts. Sci Rep. 2016;6:32993. doi: 10.1038/srep32993. PubMed PMID: 27615560; PubMed Central PMCID: PMCPMC5018733.
29. Bateman A, Cheung ST, Bennett HPJ. A Brief Overview of Progranulin in Health and Disease. Methods Mol Biol. 2018;1806:3-15. Epub 2018/06/30. doi: 10.1007/978-1-4939-8559-3_1. PubMed PMID: 29956265.
30. Yokoyama T, Komori A, Nakamura M, Takii Y, Kamihira T, Shimoda S, et al. Human intrahepatic biliary epithelial cells function in innate immunity by producing IL-6 and IL-8 via the TLR4-NF-kappaB and -MAPK signaling pathways. Liver Int. 2006;26(4):467-76. doi: 10.1111/j.1478-3231.2006.01254.x. PubMed PMID: 16629651.
31. Upontain S, Sereerak P, Laha T, Sripa B, Tangkawatana P, Brindley PJ, et al. Granulin Expression in Hamsters during Opisthorchis viverrini Infection-Induced Cholangiocarcinogenesis. Asian Pac J Cancer Prev. 2018;19(9):2437-45. doi: 10.22034/APJCP.2018.19.9.2437. PubMed PMID: 30255697; PubMed Central PMCID: PMCPMC6249462.
32. Kiguchi K, Carbajal S, Chan K, Beltran L, Ruffino L, Shen J, et al. Constitutive expression of ErbB-2 in gallbladder epithelium results in development of adenocarcinoma. Cancer Res. 2001;61(19):6971-6. PubMed PMID: 11585718.
33. Andersen JB. Molecular pathogenesis of intrahepatic cholangiocarcinoma. J Hepatobiliary Pancreat Sci. 2015;22(2):101-13. doi: 10.1002/jhbp.155. PubMed PMID: 25174625.
34. Churi CR, Shroff R, Wang Y, Rashid A, Kang HC, Weatherly J, et al. Mutation profiling in cholangiocarcinoma: prognostic and therapeutic implications. PLoS One. 2014;9(12):e115383. doi: 10.1371/journal.pone.0115383. PubMed PMID: 25536104; PubMed Central PMCID: PMCPMC4275227.
35. Ross JS, Wang K, Gay L, Al-Rohil R, Rand JV, Jones DM, et al. New routes to targeted therapy of intrahepatic cholangiocarcinomas revealed by next-generation sequencing. Oncologist. 2014;19(3):235-42. doi: 10.1634/theoncologist.2013-0352. PubMed PMID: 24563076; PubMed Central PMCID: PMCPMC3958461.
36. Loilome W, Bungkanjana P, Techasen A, Namwat N, Yongvanit P, Puapairoj A, et al. Activated macrophages promote Wnt/beta-catenin signaling in cholangiocarcinoma cells.

Tumour Biol. 2014;35(6):5357-67. doi: 10.1007/s13277-014-1698-2. PubMed PMID: 24549785; PubMed Central PMCID: PMCPMC4862210.

37. Dokduang H, Juntana S, Techasen A, Namwat N, Yongvanit P, Khuntikeo N, et al. Survey of activated kinase proteins reveals potential targets for cholangiocarcinoma treatment. Tumour Biol. 2013;34(6):3519-28. doi: 10.1007/s13277-013-0930-9. PubMed PMID: 23812726.

38. Loilome W, Juntana S, Namwat N, Bhudhisawasdi V, Puapairoj A, Sripa B, et al. PRKAR1A is overexpressed and represents a possible therapeutic target in human cholangiocarcinoma. Int J Cancer. 2011;129(1):34-44. doi: 10.1002/ijc.25646. PubMed PMID: 20824711.

39. Yothaisong S, Thanee M, Namwat N, Yongvanit P, Boonmars T, Puapairoj A, et al. Opisthorchis viverrini infection activates the PI3K/ AKT/PTEN and Wnt/beta-catenin signaling pathways in a Cholangiocarcinogenesis model. Asian Pac J Cancer Prev. 2014;15(23):10463-8. PubMed PMID: 25556493.

40. Chen BH, Gilbert LA, Cimini BA, Schnitzbauer J, Zhang W, Li GW, et al. Dynamic Imaging of Genomic Loci in Living Human Cells by an Optimized CRISPR/Cas System. Cell. 2013;155(7):1479-91. doi: 10.1016/j.cell.2013.12.001. PubMed PMID: ISI:000328693300006.

41. Zhang QY, Men CJ, Ding XW. Upregulation of microRNA-140-3p inhibits epithelial-mesenchymal transition, invasion, and metastasis of hepatocellular carcinoma through inactivation of the MAPK signaling pathway by targeting GRN. J Cell Biochem. 2019. doi: 10.1002/jcb.28750. PubMed PMID: 31044454.

42. Engel NW, Neumann JE, Ahlfeld J, Wefers AK, Merk DJ, Ohli J, et al. Canonical Wnt Signaling Drives Tumor-Like Lesions from Sox2-Positive Precursors of the Murine Olfactory Epithelium. PLoS One. 2016;11(11):e0166690. doi: 10.1371/journal.pone.0166690. PubMed PMID: 27902722; PubMed Central PMCID: PMCPMC5130221.

43. Schnerch A, Cerdan C, Bhatia M. Distinguishing between mouse and human pluripotent stem cell regulation: the best laid plans of mice and men. Stem Cells. 2010;28(3):419-30. doi: 10.1002/stem.298. PubMed PMID: 20054863.

44. Sui L, Bouwens L, Mfopou JK. Signaling pathways during maintenance and definitive endoderm differentiation of embryonic stem cells. Int J Dev Biol. 2013;57(1):1-12. doi: 10.1387/ijdb.120115ls. PubMed PMID: 23585347.

45. Brennan DJ, Ek S, Doyle E, Drew T, Foley M, Flannelly G, et al. The transcription factor Sox11 is a prognostic factor for improved recurrence-free survival in epithelial ovarian cancer. Eur J Cancer. 2009;45(8):1510-7. doi: 10.1016/j.ejca.2009.01.028. PubMed PMID: 19272768.

46. Kuci V, Nordstrom L, Conrotto P, Ek S. SOX11 and HIG-2 are cross-regulated and affect growth in mantle cell lymphoma. Leuk Lymphoma. 2016;57(8):1883-92. doi: 10.3109/10428194.2015.1121257. PubMed PMID: 26757780.

47. Kuci V, Nordstrom L, Jerkeman M, Ek S. Emerging role of SOX11 in mantle cell lymphoma. Blood and Lymphatic Cancer: Targets and Therapy. 2015;2015(5): 35-42.

48. Ninlawan K, O'Hara SP, Splinter PL, Yongvanit P, Kaewkes S, Surapaitoon A, et al. Opisthorchis viverrini excretory/secretory products induce toll-like receptor 4 upregulation and production of interleukin 6 and 8 in cholangiocyte. Parasitol Int. 2010;59(4):616-21. Epub 2010/10/05. doi: 10.1016/j.parint.2010.09.008. PubMed PMID: 20887801; PubMed Central PMCID: PMCPMC3319364.

49. Grubman SA, Perrone RD, Lee DW, Murray SL, Rogers LC, Wolkoff LI, et al. Regulation of intracellular pH by immortalized human intrahepatic biliary epithelial cell lines.

Am J Physiol. 1994;266(6 Pt 1):G1060-70. Epub 1994/06/01. doi: 10.1152/ajpgi.1994.266.6.G1060. PubMed PMID: 8023938.

50. Ittiprasert W, Mann VH, Karinshak SE, Coghlan A, Rinaldi G, Sankaranarayanan G, et al. Programmed genome editing of the omega-1 ribonuclease of the blood fluke, Schistosoma mansoni. Elife. 2019;8. Epub 2019/01/16. doi: 10.7554/eLife.41337. PubMed PMID: 30644357; PubMed Central PMCID: PMCPMC6355194.

51. Telenti A, Pierce LC, Biggs WH, di Iulio J, Wong EH, Fabani MM, et al. Deep sequencing of 10,000 human genomes. Proc Natl Acad Sci U S A. 2016;113(42):11901-6. doi: 10.1073/pnas.1613365113. PubMed PMID: 27702888; PubMed Central PMCID: PMCPMC5081584.

52. Canver MC, Haeussler M, Bauer DE, Orkin SH, Sanjana NE, Shalem O, et al. Integrated design, execution, and analysis of arrayed and pooled CRISPR genome-editing experiments. Nat Protoc. 2018;13(5):946-86. Epub 2018/04/14. doi: 10.1038/nprot.2018.005. PubMed PMID: 29651054; PubMed Central PMCID: PMCPMC6182299.

53. Anthis NJ, Clore GM. Sequence-specific determination of protein and peptide concentrations by absorbance at 205 nm. Protein Sci. 2013;22(6):851-8. Epub 2013/03/26. doi: 10.1002/pro.2253. PubMed PMID: 23526461; PubMed Central PMCID: PMCPMC3690723.

54. Santos JC, Lima NDS, Sarian LO, Matheu A, Ribeiro ML, Derchain SFM. Exosome-mediated breast cancer chemoresistance via miR-155 transfer. Sci Rep. 2018;8(1):829. Epub 2018/01/18. doi: 10.1038/s41598-018-19339-5. PubMed PMID: 29339789; PubMed Central PMCID: PMCPMC5770414.

55. Shenoy GN, Loyall J, Berenson CS, Kelleher RJ, Jr., Iyer V, Balu-Iyer SV, et al. Sialic Acid-Dependent Inhibition of T Cells by Exosomal Ganglioside GD3 in Ovarian Tumor Microenvironments. J Immunol. 2018;201(12):3750-8. Epub 2018/11/18. doi: 10.4049/jimmunol.1801041. PubMed PMID: 30446565; PubMed Central PMCID: PMCPMC6289713.

56. Betker JL, Angle BM, Graner MW, Anchordoquy TJ. The Potential of Exosomes From Cow Milk for Oral Delivery. J Pharm Sci. 2019;108(4):1496-505. Epub 2018/11/24. doi: 10.1016/j.xphs.2018.11.022. PubMed PMID: 30468828.

57. Livak KJ, Schmittgen TD. Analysis of relative gene expression data using real-time quantitative PCR and the 2(-Delta Delta C(T)) Method. Methods. 2001;25(4):402-8. Epub 2002/02/16. doi: 10.1006/meth.2001.1262. PubMed PMID: 11846609.

58. Bradford MM. A rapid and sensitive method for the quantitation of microgram quantities of protein utilizing the principle of protein-dye binding. Anal Biochem. 1976;72:248-54. Epub 1976/05/07. PubMed PMID: 942051.

59. Garnier D, Magnus N, Lee TH, Bentley V, Meehan B, Milsom C, et al. Cancer cells induced to express mesenchymal phenotype release exosome-like extracellular vesicles carrying tissue factor. J Biol Chem. 2012;287(52):43565-72. Epub 2012/11/03. doi: 10.1074/jbc.M112.401760. PubMed PMID: 23118232; PubMed Central PMCID: PMCPMC3527943.

60. Puzar Dominkus P, Stenovec M, Sitar S, Lasic E, Zorec R, Plemenitas A, et al. PKH26 labeling of extracellular vesicles: Characterization and cellular internalization of contaminating PKH26 nanoparticles. Biochim Biophys Acta Biomembr. 2018;1860(6):1350-61. Epub 2018/03/20. doi: 10.1016/j.bbamem.2018.03.013. PubMed PMID: 29551275.

61. Tario JD, Jr., Humphrey K, Bantly AD, Muirhead KA, Moore JS, Wallace PK. Optimized staining and proliferation modeling methods for cell division monitoring using cell

tracking dyes. J Vis Exp. 2012;(70):e4287. Epub 2012/12/29. doi: 10.3791/4287. PubMed PMID: 23271219; PubMed Central PMCID: PMCPMC3673170.

62. von Kleist L, Stahlschmidt W, Bulut H, Gromova K, Puchkov D, Robertson MJ, et al. Role of the clathrin terminal domain in regulating coated pit dynamics revealed by small molecule inhibition. Cell. 2011;146(3):471-84. Epub 2011/08/06. doi: 10.1016/j.cell.2011.06.025. PubMed PMID: 21816279.

63. Heallen T, Zhang M, Wang J, Bonilla-Claudio M, Klysik E, Johnson RL, et al. Hippo pathway inhibits Wnt signaling to restrain cardiomyocyte proliferation and heart size. Science. 2011;332(6028):458-61. Epub 2011/04/23. doi: 10.1126/science.1199010. PubMed PMID: 21512031; PubMed Central PMCID: PMCPMC3133743.

64. Yasuda K, Hirohashi Y, Kuroda T, Takaya A, Kubo T, Kanaseki T, et al. MAPK13 is preferentially expressed in gynecological cancer stem cells and has a role in the tumor-initiation. Biochem Biophys Res Commun. 2016;472(4):643-7. Epub 2016/03/13. doi: 10.1016/j.bbrc.2016.03.004. PubMed PMID: 26969274.

65. Weigle B, Ebner R, Temme A, Schwind S, Schmitz M, Kiessling A, et al. Highly specific overexpression of the transcription factor SOX11 in human malignant gliomas. Oncol Rep. 2005;13(1):139-44. Epub 2004/12/08. PubMed PMID: 15583815.

66. Rasti M, Honardar Z, Nikseresht M, Owji A. Quantitative Analysis of ErbB1 and ErbB2 Genes Amplification by a High Performance Liquid Chromatography. Avicenna J Med Biotechnol. 2014;6(4):228-37. Epub 2014/11/22. PubMed PMID: 25414785; PubMed Central PMCID: PMCPMC4224662.

67. Gilbert-Sirieix M, Makoukji J, Kimura S, Talbot M, Caillou B, Massaad C, et al. Wnt/beta-catenin signaling pathway is a direct enhancer of thyroid transcription factor-1 in human papillary thyroid carcinoma cells. PLoS One. 2011;6(7):e22280. Epub 2011/08/05. doi: 10.1371/journal.pone.0022280. PubMed PMID: 21814573; PubMed Central PMCID: PMCPMC3141030.

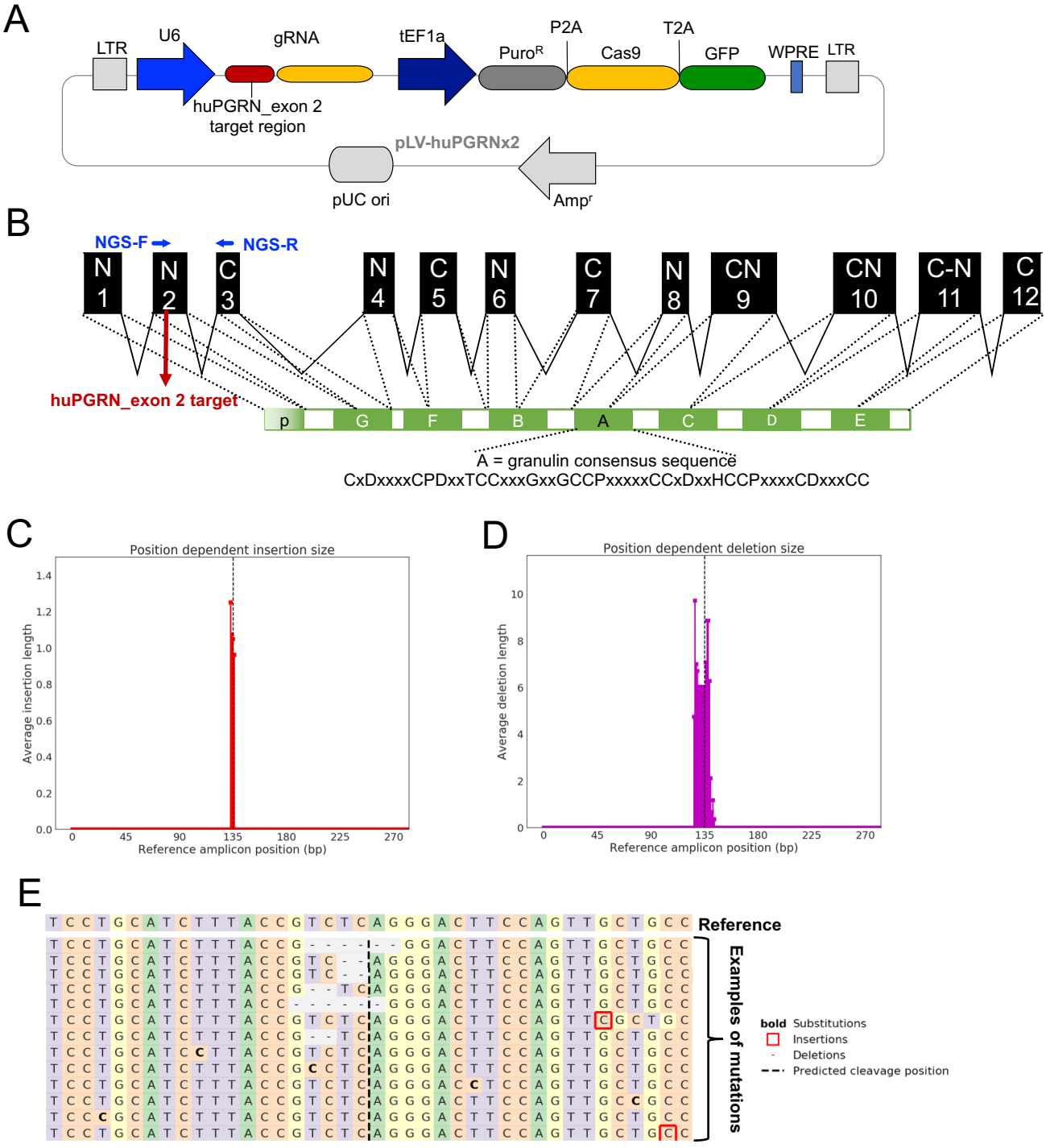
A
LTR
U6
gRNA
huPGRN_exon 2
target region
tEF1a
Puro^R
P2A
Cas9
T2A
GFP
WPRE
LTR
pLV-huPGRNx2
pUC ori
Amp^r
B
NGS-F
NGS-R
N 1
N 2
C 3
N 4
C 5
N 6
C 7
N 8
CN 9
CN 10
C-N 11
C 12
huPGRN_exon 2 target
p
G
F
B
A
C
D
E
A = granulin consensus sequence
CxDxxxxCPDxxTCCxxxGxxGCCPxxxxxCCxDxxHCCPxxxxCDxxxCC
C
Position dependent insertion size
Average insertion length
Reference amplicon position (bp)
D
Position dependent deletion size
Average deletion length
Reference amplicon position (bp)
E
Reference
Examples of mutations
bold Substitutions
Insertions
Deletions
Predicted cleavage position

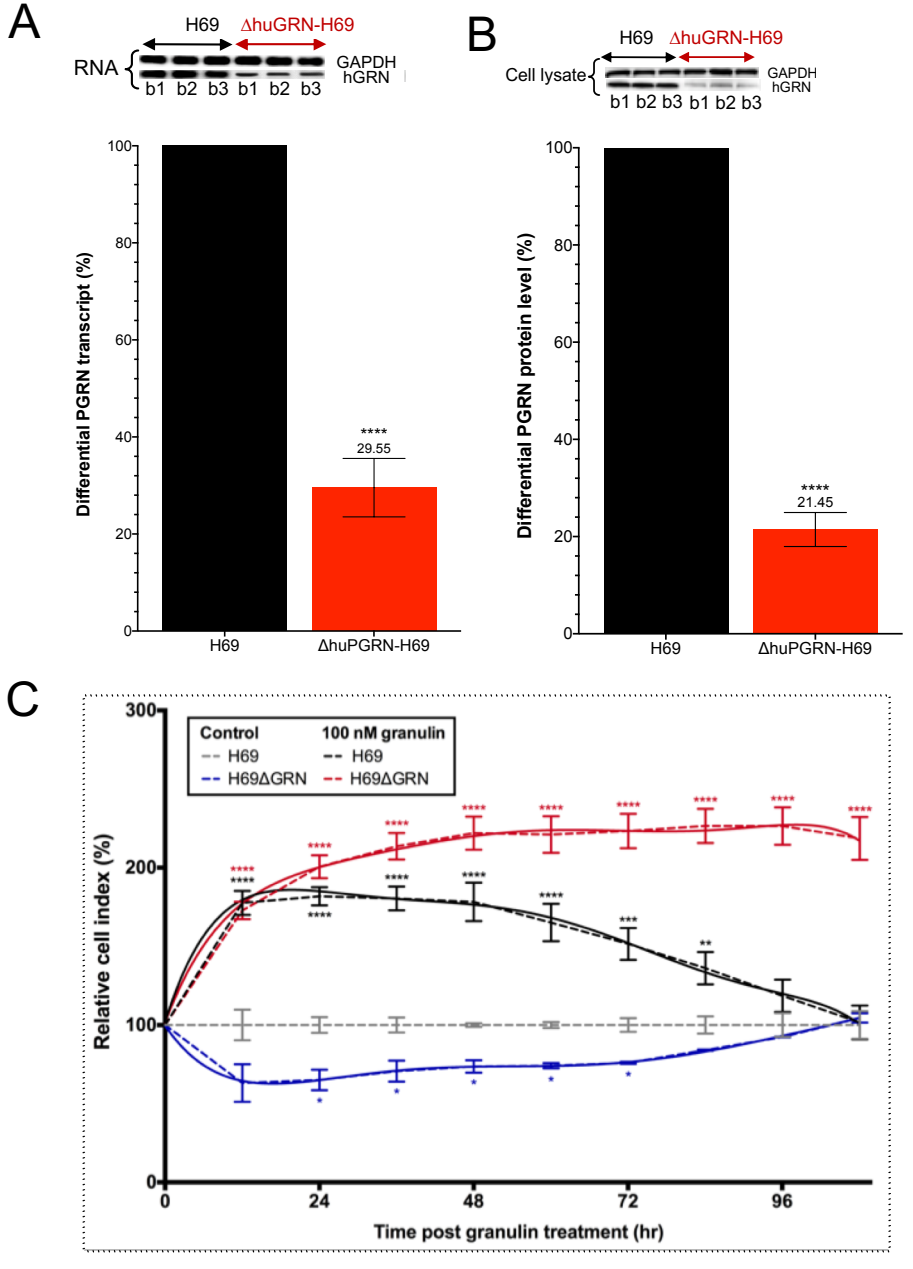
A
H69
ΔhuGRN-H69
RNA
GAPDH
hGRN
b1 b2 b3 b1 b2 b3
Differential PGRN transcript (%)
100
80
60
40
20
0
****
29.55
H69
ΔhuPGRN-H69
B
H69
ΔhuGRN-H69
Cell lysate
GAPDH
hGRN
b1 b2 b3 b1 b2 b3
Differential PGRN protein level (%)
100
80
60
40
20
0
****
21.45
H69
ΔhuPGRN-H69
C
Control
100 nM granulin
H69
H69ΔGRN
H69
H69ΔGRN
Relative cell index (%)
300
200
100
0
0
24
48
72
96
Time post granulin treatment (hr)

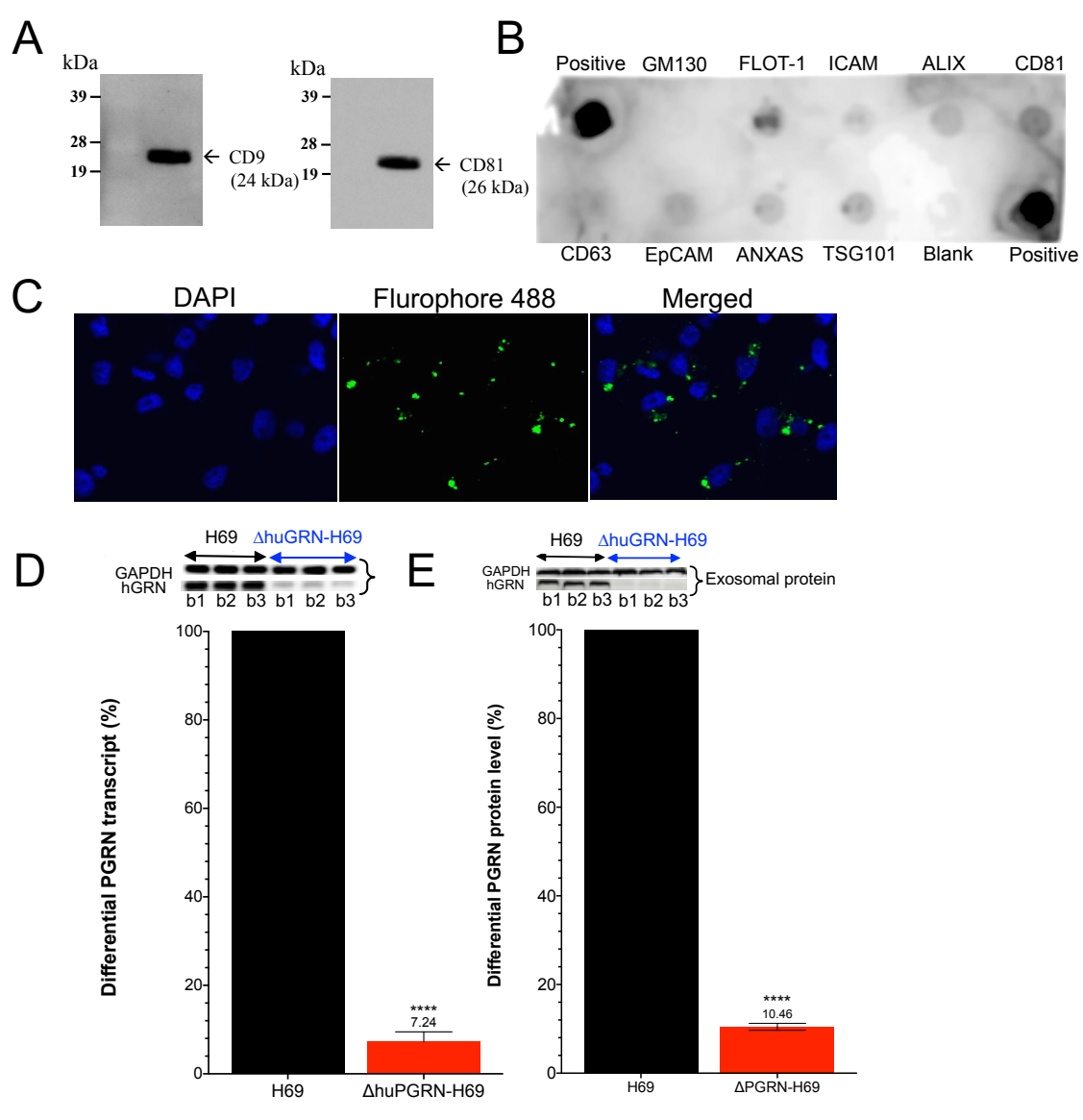
A
kDa
39
28
19
CD9
(24 kDa)
kDa
39
28
19
CD81
(26 kDa)
B
Positive
GM130
FLOT-1
ICAM
ALIX
CD81
CD63
EpCAM
ANXAS
TSG101
Blank
Positive
C
DAPI
Flurophore 488
Merged
D
H69
ΔhuGRN-H69
GAPDH
hGRN
b1 b2 b3 b1 b2 b3
Differential PGRN transcript (%)
100
80
60
40
20
0
****
7.24
H69
ΔhuPGRN-H69
E
H69
ΔhuGRN-H69
GAPDH
hGRN
Exosomal protein
b1 b2 b3 b1 b2 b3
Differential PGRN protein level (%)
100
80
60
40
20
0
****
10.46
H69
ΔPGRN-H69

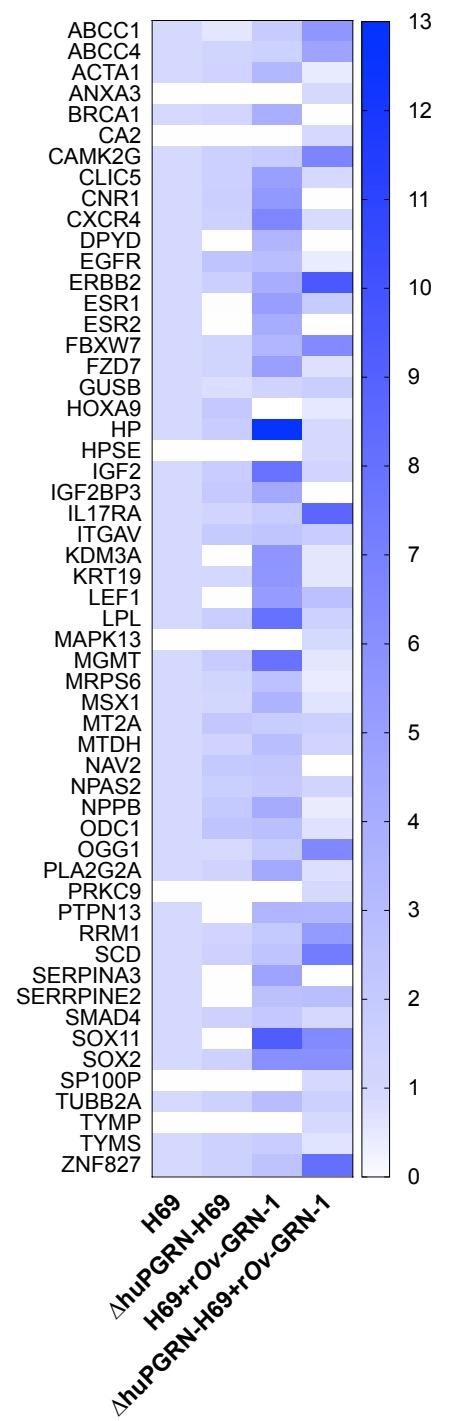
ABCC1
ABCC4
ACTA1
ANXA3
BRCA1
CA2
CAMK2G
CLIC5
CNR1
CXCR4
DPYD
EGFR
ERBB2
ESR1
ESR2
FBXW7
FZD7
GUSB
HOXA9
HP
HPSE
IGF2
IGF2BP3
IL17RA
ITGAV
KDM3A
KRT19
LEF1
LPL
MAPK13
MGMT
MRPS6
MSX1
MT2A
MTDH
NAV2
NPAS2
NPPB
ODC1
OGG1
PLA2G2A
PRKC9
PTPN13
RRM1
SCD
SERPINA3
SERRPINE2
SMAD4
SOX11
SOX2
SP100P
TUBB2A
TYMP
TYMS
ZNF827
13
12
11
10
9
8
7
6
5
4
3
2
1
0
H69
ΔhuPGRN-H69
H69+rOv-GRN-1
ΔhuPGRN-H69+rOv-GRN-1

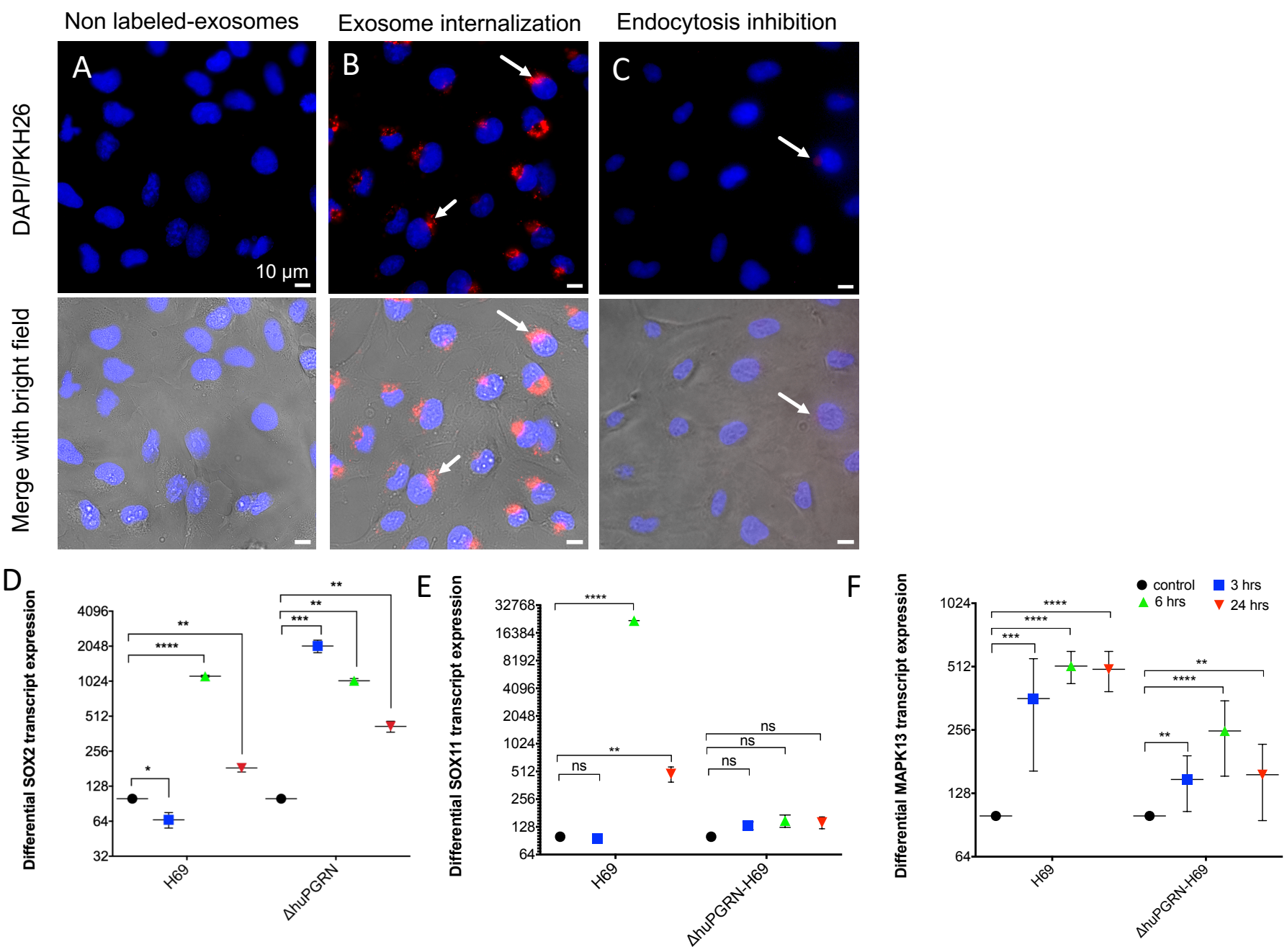
Non labeled-exosomes
Exosome internalization
Endocytosis inhibition
DAPI/PKH26
Merge with bright field
A
B
C
10 µm
D
Differential SOX2 transcript expression
4096
2048
1024
512
256
128
64
32
H69
ΔhuPGRN
E
Differential SOX11 transcript expression
32768
16384
8192
4096
2048
1024
512
256
128
64
H69
ΔhuPGRN-H69
ns
F
Differential MAPK13 transcript expression
control
3 hrs
6 hrs
24 hrs
1024
512
256
128
64
H69
ΔhuPGRN-H69